PNAS
www.pnas.org

Supplementary Information

Absence of retbindin blocks glycolytic flux, disrupts metabolic homeostasis and leads to photoreceptor degeneration

Tirthankar Sinha[1], Jianhai Du[2], Mustafa S. Makia[1], James B. Hurley[3], Muna I. Naash[1,*]and Muayyad R. Al-Ubaidi[1,*]

[1]Department of Biomedical Engineering, University of Houston, Houston, TX 77204

[2]Department of Ophthalmology and Department of Biochemistry, West Virginia University, Morgantown, WV 26506

[3]Department of Biochemistry, University of Washington, Seattle, WA98195

*To whom correspondence should be addressed at: Department of Biomedical Engineering, University of Houston, 3517 Cullen Blvd., Houston, TX 77204, USA, malubaid@central.uh.edu or mnaash@central.uh.edu, +1-713-743-1648 (MRA) and +1-713-743-1651 (MIN).

This PDF file includes:

Supplementary text
Figures S1 to S4
SI References

Supplemental Methods

Experimental Model and Subject details

Strain/Genetic makeup of mice

Animal experiments were approved by the University of Houston Institutional Animal Care and Use Committee (IACUC) and adhered to recommendations in NIH Guide for the Care and Use of Laboratory Animals and the Association for Research in Vision and Ophthalmology. All mice were on C5BL/6 background and were genotyped and found to be negative for both the rd8 allele (Chen et al., 2013) and have the RPE65 Leu450 variant (Danciger et al., 2000; Kim et al., 2004). Animals were reared under cyclic light conditions (12 hours L/D, ~30 lux) and fed normal chow (Picolab Rodent Diet 5053). The *Rtbdn*$^{-/-}$ animals were generated as previously described.

Supplemental Methods

Tissue collection

We fasted the animals for 5-6 hours to reduce the variability arising from differential feeding (1, 2) and collected samples between 1 and 3 PM. Mice were anesthetized by intramuscular injection of 85 mg/kg ketamine and 14 mg/kg xylazine. Using forceps and tweezers, the NR was extracted and the rest of the eyecup was carefully removed. The RPE-Ch was carefully scraped out of the eyecup, quickly extracted, rinsed in phosphate buffered saline (pH 7.4) and immediately frozen in liquid nitrogen. To ensure freshness of the tissue and to prevent changes during the extraction process, the entire procedure was completed within 2-3 minutes of the animal falling under anesthesia. After the samples were collected, the animals were euthanized via carbon dioxide inhalation. All samples were thereafter maintained at -80ºC until processed. Six retinas and corresponding six RPE-Chs from six non-littermate animals were pooled and considered as a single metabolomic measurement for the NR and for the RPE-Ch presented in Fig. 2 and from 6 independent measurements (n=6) for each. However, the metabolomic data presented in *SI Appendix*, Fig. S3 was generated from a combination of two retinas and two associated RPE-Ch from a single animal and from 3 independent measurements (n=3).

Histological and functional assessments

Light histology and morphometry

Eyes were enucleated and fixed in 2% glutaraldehyde, 2% paraformaldehyde, 100 mM cacodylate, 0.025% CaCl2 (3). Eyes were embedded in plastic resin and sectioned as previously described

(4). Images at the light microscopy were captured at 40X and stained with 2% (v/v) uranyl acetate and Reynold's lead citrate. Images shown in Fig. S1B were captured with a Zeiss Axioskop 50. For morphometrical assessments, eyes from three WT and *Rtbdn*$^{-/-}$ animals at P45 and P120 were harvested, fixed in Davidson's fixative, and embedded in paraffin as described in (5). Paraffin sections were cut along the superior-inferior plane through optic nerve and stained with hematoxylin (MHS16, Sigma, Burlington, MA, USA) and eosin (HT110116, Sigma, USA). The slides were mounted using permount mounting medium (SP15100, Fisher Scientific), and light microscopic images presented in the figures were captured using 40X objective from the inferior side, ~300 μm away from the optic nerve using a Zeiss Axioskop 50. For quantifications, cells in the outer nuclear layer were counted in 100 μm windows at intervals of 500 μm across the superior-inferior plane using ImageJ.

Electroretinography

Full field ERG was performed on dark-adapted WT and *Rtbdn*$^{-/-}$ animals at P45 and P120 as described previously (6) using UTAS system (LKC, Gaithersburg, MD, USA). Eyes of anesthetized animals were dilated with 1% cyclopentolate for five minutes, and then a single drop of Gonak (2.5% hypromellose) was applied and platinum wire loop electrodes were placed on the eyes. Scotopic electroretinography (ERG) was recorded in response to a single flash of white light at the 157.7 cd s/m2. After 5 min light adaptation (29.03 cd/m2), photopic ERGs were recorded in response to 25 flashes at 79 cd s/m2 intensity. ERG waveforms are shown in Fig. S1A.

Tissue Extraction and metabolomics analyses

Extraction of the samples as explained below was performed by Metabolon, Inc. (Morrisville, NC, USA). Several recovery standards were added prior to the first step in the extraction process for quality control purposes. In order to increase maximum yield, methanol extraction was done prior to analysis. To remove proteins, dissociate small molecules bound to protein or trapped in the precipitated protein matrix, and to recover chemically diverse metabolites, proteins were precipitated with methanol under vigorous shaking for 2 min followed by centrifugation. The resulting extract was divided into five fractions: two for analysis by two separate reverse phase (RP)/UPLC-MS/MS methods with positive ion mode electrospray ionization (ESI), one for analysis by RP/UPLC-MS/MS with negative ion mode ESI, one for analysis by HILIC/UPLC-

MS/MS with negative ion mode ESI, and one sample was reserved for backup. Post removal of the organic solvent, the sample extracts were stored overnight under nitrogen before preparation for analysis.

Measurements

Metabolomics measurements were performed independently, first in-house (in JBH lab) for a lower n value (n=3) and then and at Metabolon, Inc (Morrisville, NC, USA) with a larger n value (n=6) and more expansive library to metabolite detection. Both data were found to be similar, but because of the platform differences between the two methods, metabolomics measurement from the initial study (n=3) is only shown in *SI Appendix*, Fig. S3, while the data shown in Fig. 1, 2, 4, and *SI Appendix*, Fig. S4 are obtained as performed through Metabolon, Inc (Morrisville, NC, USA). Measurement as explained below was performed by Metabolon, Inc. (Morrisville, NC, USA). All methods utilized a Waters ACQUITY ultra-performance liquid chromatography (UPLC) and a Thermo Scientific Q-Exactive high resolution/accurate mass spectrometer interfaced with a heated electrospray ionization (HESI-II) source and Orbitrap mass analyzer operated at 35,000 mass resolution. The sample extract was first dried and then reconstituted in solvents compatible to each of the four methods as mentioned. Each reconstitution solvent contained a series of standards at fixed concentrations to ensure injection and chromatographic consistency. One aliquot was analyzed using acidic positive ion conditions, chromatographically optimized for more hydrophilic compounds. In this method, the extract was gradient eluted from C18 column (Waters UPLC BEH C18-2.1 x 100 mm, 1.7 µm) using water and methanol, containing 0.05% perfluoropentanoic acid (PFPA) and 0.1% formic acid (FA). Another aliquot was also analyzed using acidic positive ion conditions; however, it was chromatographically optimized for more hydrophobic compounds. In this method, the extract was gradient eluted from the same afore mentioned C18 column using methanol, acetonitrile, water, 0.05% PFPA and 0.01% FA and was operated at an overall higher organic content. Another aliquot was analyzed using basic negative ion optimized conditions using a separate dedicated C18 column. The basic extracts were eluted as gradient from the column using methanol and water, however with 6.5mM Ammonium Bicarbonate at pH 8. The fourth aliquot was then analyzed via negative ionization following elution from a HILIC column (Waters UPLC BEH Amide 2.1x150 mm, 1.7 µm) using a gradient consisting of water and acetonitrile with 10mM Ammonium Formate, pH 10.8. The

MS analysis alternated between MS and data-dependent MS^n scans using dynamic exclusion. The scan range varied slighted between methods but covered 70-1000 m/z. Compounds were identified by comparing to respective library entries of purified standards or recurrent unknown entities. Peaks were then quantified by measurement of respective area-under-the-curve. For studies that span for multiple days, a data normalization step was performed to correct for the variation resulting from instrument inter-day tuning differences. Biochemical data for each metabolite was then normalized to the protein concentration as measured by Bradford assay to account for differences in metabolite levels due to differences in the amount of material present in each sample.

Quality Control

Along with the experimental samples, various types of control samples were analyzed: a pooled matrix sample generated by taking a small volume of each experimental sample served as a technical replicate throughout the data set; extracted water samples served as process blanks; and a cocktail of quality control standards that were carefully chosen not to interfere with the measurement of endogenous compounds were spiked into every analyzed sample, allowed instrument performance monitoring and aided chromatographic alignment. Instrument variability was measured by calculating the median relative standard deviation (RSD) for the internal standards that were added to each sample prior to injection into the mass spectrometers. Overall process variability was measured by calculating the median RSD for all endogenous metabolites (i.e., non-instrument standards) present in 100% of the technical replicates of pooled samples. Internal standards reflected instrument variability of only 6% median RSD, while endogenous metabolites reflected a total process variability of only 2% median RSD. Experimental samples were randomized across the platform run with QC samples spaced evenly between the injections.

^{13}C labeling and measurements by GC-MS

Collected fresh neural retinas were immediately incubated in newly prepared Krebs-Ringer-Bicarbonate (KRB) buffer as an *ex vivo* culture, along with U-^{13}C-glucose (5mM) for 5 min and 45 min. Each reaction was stopped by transferring individual neural retina to cold 0.9% NaCl solution and was subsequently frozen. From each frozen sample, metabolites were derivatized by methoxymine hydrochloride followed by N-tert-butyldimethylsilyl-N-methyltrifluoroacetamide (TBDMS) as described (7). An Agilent 7890B/5977B GC/MS system with an Agilent DB-5MS

column (30 m × 0.25 mm × 0.25 µm film) was used for GC separation and analysis of metabolites. Ultra-high-purity helium was the carrier gas at a constant flow rate of 1 mL/min. One µl of sample was injected in split-less mode by the auto sampler. The temperature gradient begun at 95°C and had a hold time of 2 min and then increased at a rate of 10°C/min to 300°C, where it was held for 6 min. The temperatures were set as follows: inlet 250°C, transfer line 280°C, ion source 230°C, and quadrupole 150°C. Mass spectra were collected from 80–600 m/z under selective ion monitoring mode (8). The data was analyzed by Agilent MassHunter Quantitative Analysis Software and natural abundance was corrected by ISOCOR software.

Micro-extraction of flavins and HPLC analyese

Tissues were extracted as previously described (1). Briefly, tissues were homogenized using a handheld motor and pestle in 100µl of 1X PBS (pH 6.8 unless otherwise indicated) and a 30µl aliquot was saved for protein assay. The rest was centrifuged at 1,000Xg for 10 minutes at 4ºC and supernatant was separated and incubated at 37ºC in 10% TCA (optimized by using 5%, 10% and 25%) for 15 minutes to precipitate proteins. The tube was centrifuged at 10,000Xg for 10 minutes at 4ºC; supernatant was carefully collected, filtered through 0.45µm filter and used for HPLC analysis. To minimize any effect of freeze thaw, injection of samples into the HPLC system was done right after extraction for all the samples, without freezing them.

HPLC Chromatography

The chromatographic separation was as per previously described (1). Briefly, mobile phase used was phosphate buffer (50 mM) and at pH (3.1). The HPLC setup was composed of Waters binary HPLC pump (1525), Waters auto-sampler (2707), Waters multi wavelength fluorescence detector (2475) and a Waters X-Bridge C18 3.5µm column with dimensions of 4.6X250mm (Waters, Milford, MA, USA).

HPLC quantification of flavins

For flavin identification, a previously described method was followed (1).

Quantification and statistical analyses

Data Transformation

After log transformation and imputation of missing values, if any, with the minimum observed value for each compound, ANOVA contrasts were used to identify metabolites that differed significantly ($p \leq 0.05$), between experimental groups. An estimate of the false discovery rate (q-value) was also calculated to take into account the multiple comparisons that normally occur in metabolomic-based studies.

Data visualization

Feature scaling was done for each metabolite across all groups to set the median equal to 1. For data visualization, scatter plot was used so that the individual measurements can be seen. All data were normalized to protein levels as described in the method section. In the graphs presented in results for individual metabolites, the unit of y-axis used was "metabolite abundance" and this reflects the normalized metabolite concentration for the individual metabolite as has been reported by others (2, 9). However, for graphs representing ratios of metabolites, it was referred to as "metabolite ratio". For both individual metabolites and ratios of metabolites, values were presented for *Rtbdn*$^{-/-}$ as percent of age matched WT (red dotted line is set at 100).

Analysis of PKM2 oligomers

Two retinas from each animal and from a total of 6 animals (n=6) were collected from the respective animals and immediately (snap-freeze was avoided) homogenized in RIPA buffer using a hand-held homogenizer on ice in presence of protease inhibitors and kept on ice for an hour. Subsequently it was briefly centrifuged to pellet the insoluble material and protein concentration was determined from the supernatant via Bradford assay. Three blots were ran separately, each consisted of two WT and two *Rtbdn*$^{-/-}$ retinal extracts (15µg each), and performed under non-reducing SDS-PAGE. The respective immunoblots were probed with anti-PKM2 (CS04661) (1:1000) and anti-actin antibodies (10). Chemi-luminescence imaging of the three immunoblots were done at increasing exposure times (increment of 30 second) to identify the individual oligomers on the same immunoblot. Densitometric analysis was done of multiple exposures (till 1200 seconds) to quantify the presence of the respective bands (n=6 for WT and *Rtbdn*$^{-/-}$). PKM2 monomer and dimer saturated in early and medium exposures, respectively, while tetramer took longer exposure to be saturated on the same immunoblot.

Supplemental Figures and Legends

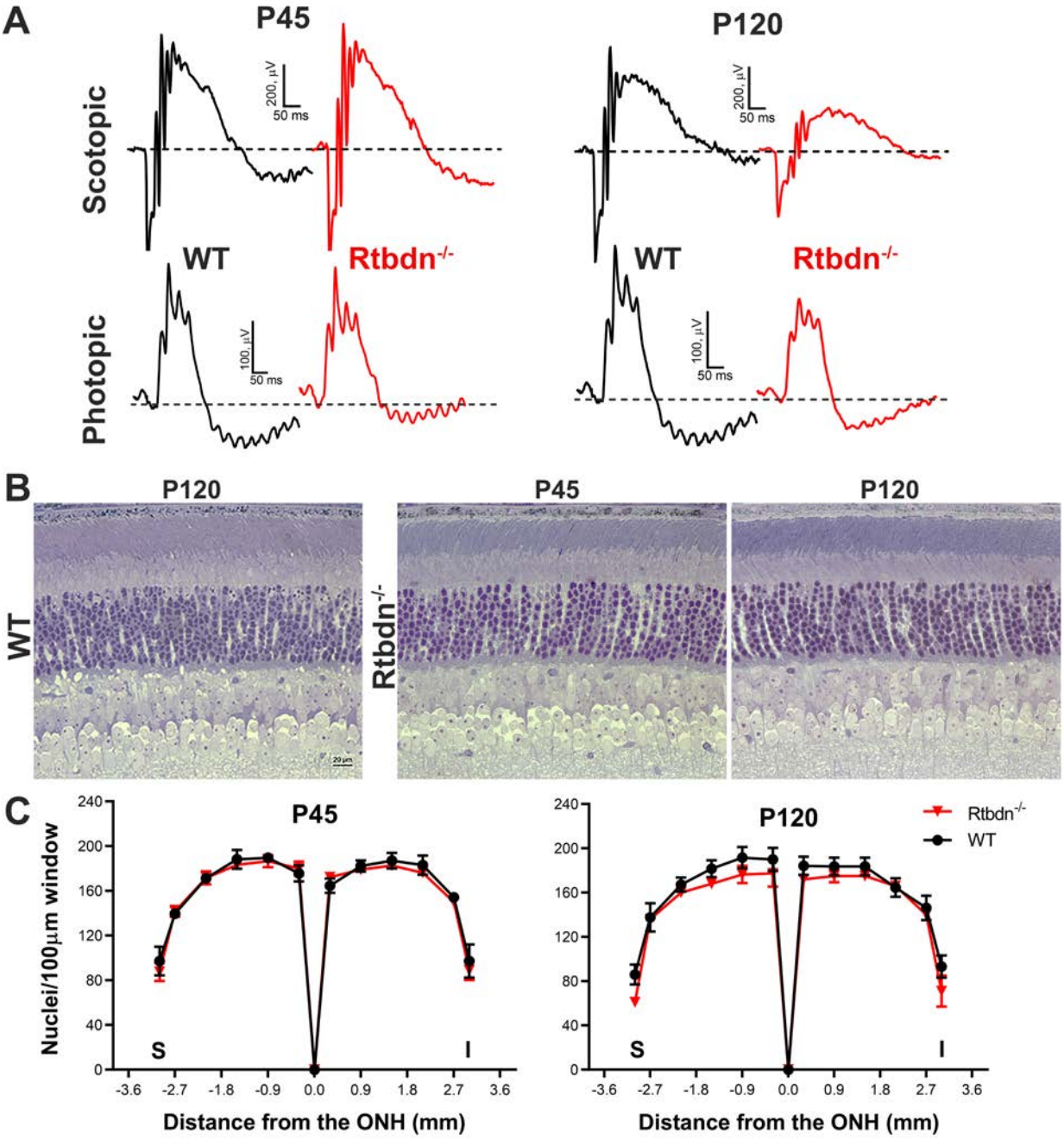

Fig. S1. RTBDN ablation leads to late onset functional and structural declines. (**A**) Shown are representative scotopic and photopic waveforms recorded at P45 and P120 of the indicated genotypes. (**B**) Representative light microscopic images of plastic embedded sections stained with toluidine blue and taken from WT and *Rtbdn*$^{-/-}$ animals at P45 and P120 of the indicated genotypes. (**C**) Photoreceptor nuclei were counted from paraffin sections across the superior-inferior plane taken from WT and *Rtbdn*$^{-/-}$ retinas at P45 and P120 and plotted in spidergrams (n=3 eyes/genotype). Although, no significant differences in photoreceptor cell count were detected at P45 and P120 between genotypes, a slight reduction in number of photoreceptor nuclei in the *Rtbdn*$^{-/-}$ retina is observed at P120.

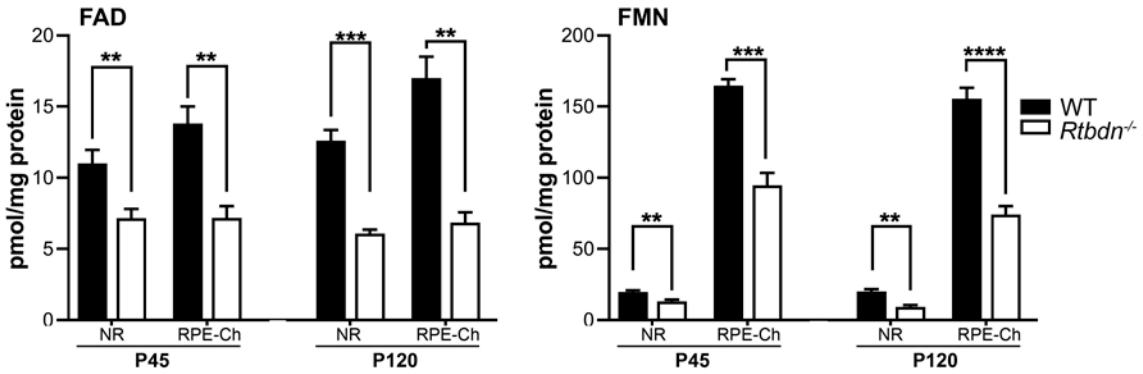

Fig. S2. Quantification of FAD and FMN in the *Rtbdn*$^{-/-}$ retina. Both FAD and FMN were quantified in the neural retina (NR) and RPE-Ch at P45 and P120. Tissues were collected as indicated in the Method Section with n=10. Student's t test was used to determine significance with **p<0.01, ***p<0.001 and ****p<0.0001.

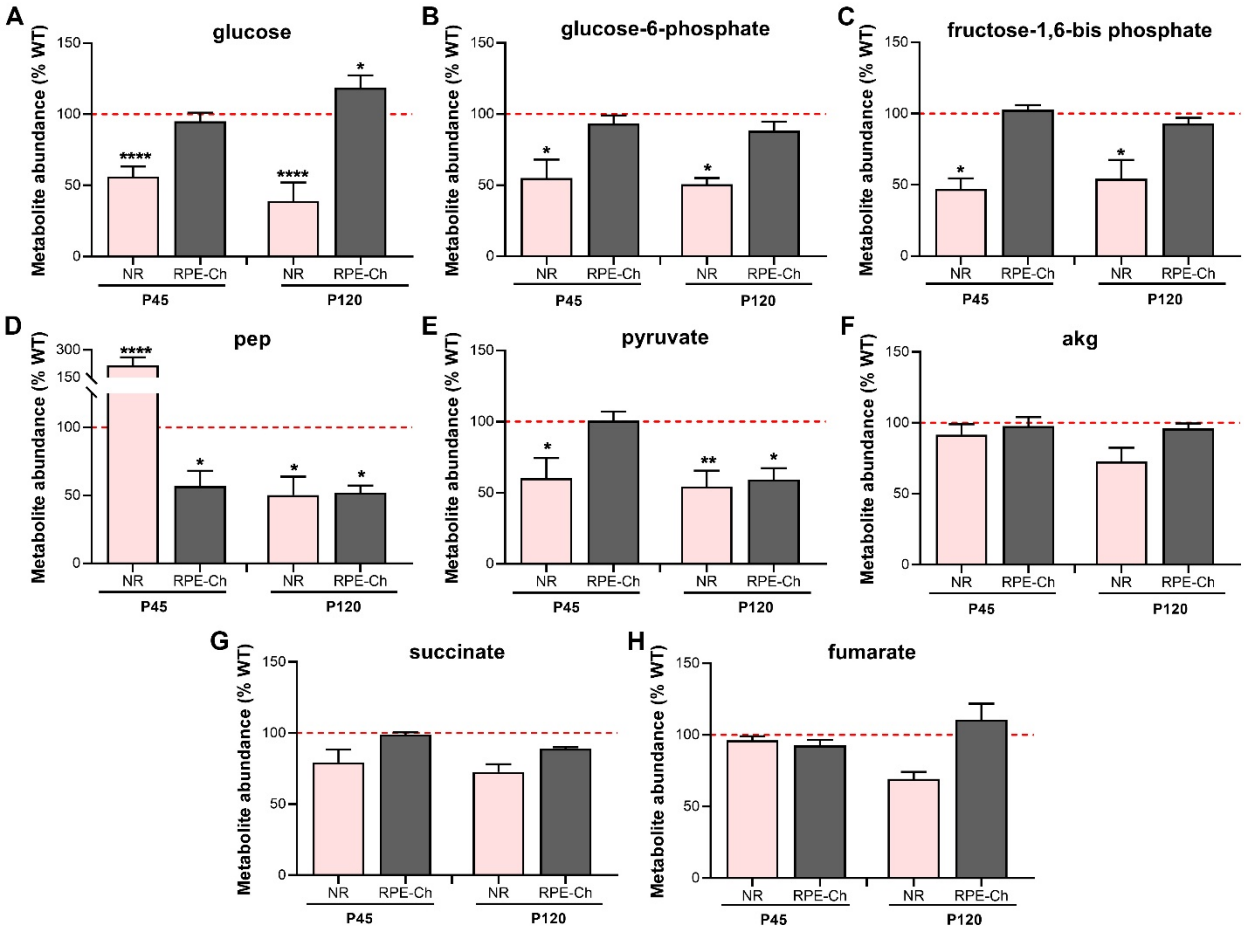

Fig. S3. Impaired steady state metabolism in absence of RTBDN. Steady state levels of key glycolytic (**A-E**) and TCA cycle (**F-H**) metabolites were quantified in NR and RPE-Ch *Rtbdn*$^{-/-}$ and WT controls at P45 and P120. Tissues were collected as indicated in the Method Section with n=3. The unit of y-axis as metabolite abundance reflects the normalized metabolite concentration for the individual metabolite. Values are presented for *Rtbdn*$^{-/-}$ as percent of age matched WT (red dotted line is set at 100). Statistical comparisons shown were made between the WT and *Rtbdn*$^{-/-}$ for the individual metabolite of each tissue at the respective ages. Student's t test was used to test significance with *p<0.05, **p<0.01, ***p<0.001 and ****p<0.0001. (NR=neural retina; RPE-Ch=RPE-Choroid).

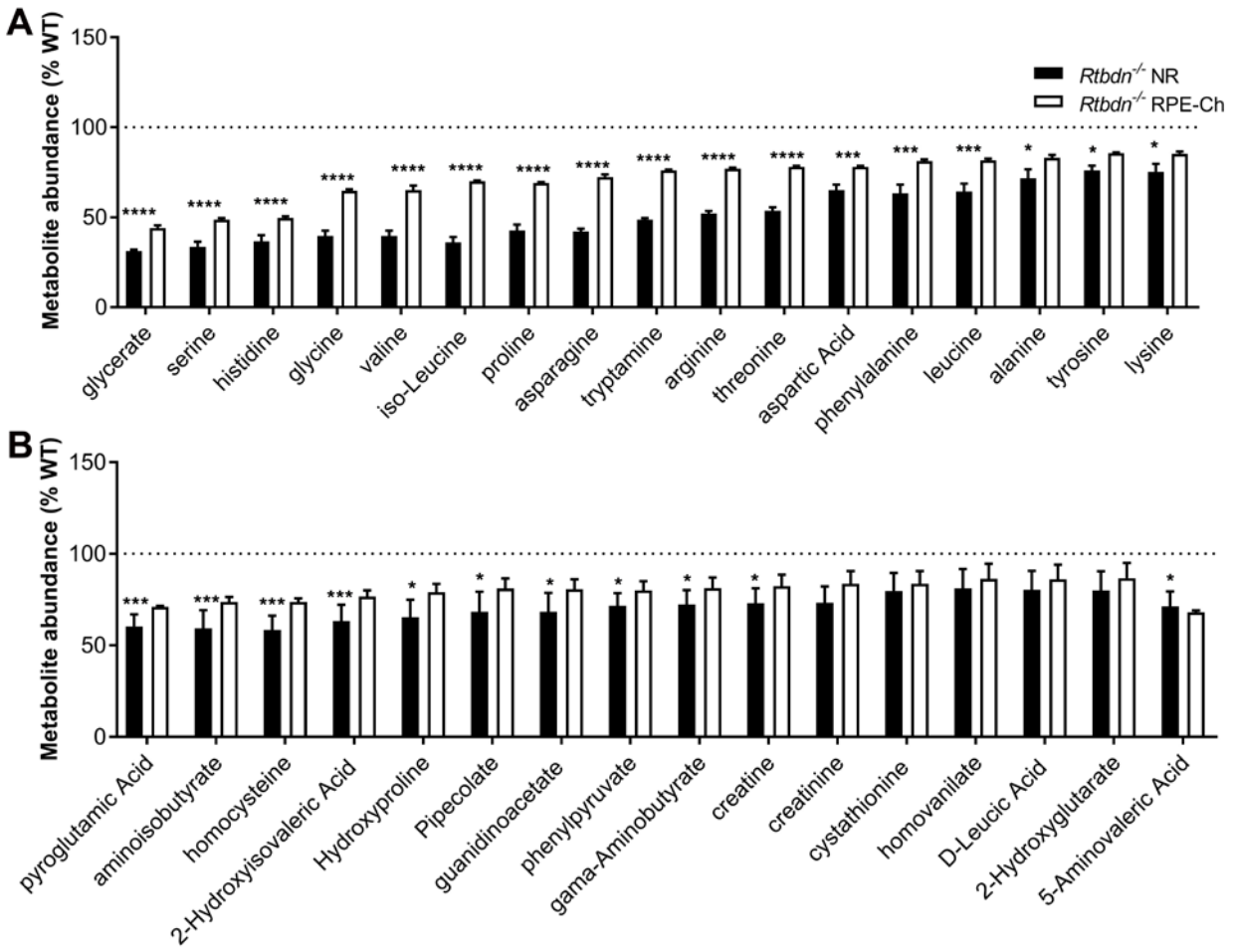

Fig. S4. Amino acid metabolism intermediates in the *Rtbdn*$^{-/-}$ and WT at P120 retina. (**A**) Key amino acids were quantified in P120 *Rtbdn*$^{-/-}$ for both neural retina (NR) and RPE-Ch and shown as percentage of the respective WT (marked as 100 percentage by dotted line). (**B**) Key amino acid metabolic intermediates were quantified in P120 *Rtbdn*$^{-/-}$ for both NR and RPE-Ch and shown as percentage of the respective WT (marked as 100 percentage by dotted line). Tissues were collected as indicated in the Method Section with n=6 for A&B. Two way ANNOVA was used to determine significance with *$p<0.05$, ***$p<0.001$ and ****$p<0.0001$.

References

1. T. Sinha, M. Makia, J. Du, M. I. Naash, M. R. Al-Ubaidi, Flavin homeostasis in the mouse retina during aging and degeneration. *J Nutr Biochem* **62**, 123-133 (2018).
2. T. Sinha, M. I. Naash, M. R. Al-Ubaidi, The symbiotic relationship between the neural retina and retinal pigment epithelium is supported by utilizing differential metabolic pathways. *IScience* https://doi.org/10.1016/j.isci.2020.101004 (2020).
3. A. M. Genc *et al.*, Elimination of a Retinal Riboflavin Binding Protein Exacerbates Degeneration in a Model of Cone-Rod Dystrophy. *Invest Ophthalmol Vis Sci* **61**, 17 (2020).
4. D. Chakraborty, X. Q. Ding, S. M. Conley, S. J. Fliesler, M. I. Naash, Differential requirements for retinal degeneration slow intermolecular disulfide-linked oligomerization in rods versus cones. *Hum Mol Genet* **18**, 797-808 (2009).
5. R. A. Kelley *et al.*, Ablation of the riboflavin-binding protein retbindin reduces flavin levels and leads to progressive and dose-dependent degeneration of rods and cones. *J Biol Chem* **292**, 21023-21034 (2017).
6. T. Cheng *et al.*, The effect of peripherin/rds haploinsufficiency on rod and cone photoreceptors. *J Neurosci* **17**, 8118-8128 (1997).
7. M. A. Kanow *et al.*, Biochemical adaptations of the retina and retinal pigment epithelium support a metabolic ecosystem in the vertebrate eye. *Elife* **6** (2017).
8. M. Yam *et al.*, Proline mediates metabolic communication between retinal pigment epithelial cells and the retina. *J Biol Chem* **294**, 10278-10289 (2019).
9. S. Zhu *et al.*, Impact of euthanasia, dissection and postmortem delay on metabolic profile in mouse retina and RPE/choroid. *Exp Eye Res* **174**, 113-120 (2018).
10. Y. Wang *et al.*, O-GlcNAcylation destabilizes the active tetrameric PKM2 to promote the Warburg effect. *Proc Natl Acad Sci U S A* **114**, 13732-13737 (2017).